A VARIATIONAL MODEL FOR OBJECT SEGMENTATION USING BOUNDARY INFORMATION, STATISTICAL SHAPE PRIOR AND THE MUMFORD-SHAH FUNCTIONAL

Xavier Bresson, Pierre Vandergheynst and Jean-Philippe Thiran

Signal Processing Institute (ITS),
Swiss Federal Institute of Technology (EPFL)
CH-1015 Lausanne, Switzerland
Email: {Xavier.Bresson, Pierre.Vandergheynst, JP.Thiran}@epfl.ch

ITS Technical Report 08.04, Fev 2004

ABSTRACT

In this paper, we propose a variational model to segment an object belonging to a given scale space using the active contour method, a geometric shape prior and the Mumford-Shah functional. We define an energy functional composed by three complementary terms. The first one detects object boundaries from image gradients. The second term constrains the active contour to get a shape compatible with a statistical shape model of the shape of interest. And the third part drives globally the shape prior and the active contour towards a homogeneous intensity region. The segmentation of the object of interest is given by the minimum of our energy functional. This minimum is computed with the calculus of variations and the gradient descent method that provide a system of evolution equations solved with the well-known level set method. We also prove the existence of this minimum in the space of functions with bounded variation. Applications of the proposed model are presented on synthetic and medical images.

1. INTRODUCTION AND MOTIVATIONS

During the last decade, variational methods and partial differential equations (PDEs) have been more and more used to analyse, understand and exploit properties of images in order to design powerful application techniques. Variational methods formulate an image processing or computer vision problem as an optimization problem depending on the unknown variables (which are functions) of the problem. When the optimization functional is differentiable, the calculus of variations provides a tool to find the extremum of the functional leading to a PDE whose steady state gives the solution of the imaging or vision problem. Variational methods and PDEs are well established domains of functional analysis which can offer strong frameworks to correctly formulate image processing problems. A very attractive property of these mathematical frameworks is to state well-posed problems to guarantee existence, uniqueness and regularity of solutions. Successful mathematical frameworks of functional analysis in computer vision are the theory of viscosity solutions [1] and the framework of functions with bounded variation [2, 3] which have given powerful tools to mathematically justify solutions of many image processing problems. Finally, applications of variational methods and PDEs have produced a lot of literature in image processing, computer vision and computer graphics as one can read in several books [4, 5, 6, 7, 8].

In computer vision, shape analysis is a core component towards automated vision systems. It can be decomposed into several research domains including shape modeling, shape registration, segmentation and pattern recognition. Among these research aeras, image segmentation plays an important role in computer vision since it is often the basis to many applications. Image segmentation has the global objective of determining the *semantically* important regions in images. In the variational framework, two approaches have been extensively studied in the litterature: the Mumford-Shah model and the active contour method. The first one aims at finding a partition of an image

(a) original image (b) segmented image (c) initial active contour (d) final active contour

Fig. 1. In the variational framework, image segmentation can be realized with the Mumford-Shah functional (a),(b) and the active contours method (c),(d).

into its constituent parts, which is realized by minimizing the Mumford-Shah functional [9], and the second one detects more specific parts using the model of active contours/snakes/propagating interfaces [10]. See Figure 1 as an example of segmentation. Active contour method is a powerful technique to perform segmentation of natural structures. Initially proposed by Kass *et al.* [10], active contours are evolving curves/surfaces (represented by PDEs) under a field of forces, depending on image features and intrinsic curve properties, that leads to the minimization of an objective functional. The numerical solution of PDEs in the context of propagating contours uses the powerful technique of level sets whose theoritical fundations are presented by Osher and Sethian in [11]. Level set methods are suitable for evolving interfaces since they are parameter-free and can deal with topological changes. Segmentation performances of fine real-world shapes such as medical structures in [12, 13, 14] are remarquable with the level set active contours. Despite of these great advantages, the first-generation active contours, based on image gradients, are highly sensitive to the presence of noise and poor image contrast, which can lead to bad segmentation results. To overcome this drawback, some authors have incorporated region-based evolution criteria into active contours, built from statistics and homogeneous intensity requirements [15, 16, 17, 18, 19, 20]. Yet the segmentation of *structures of interest* with these second-generation active contours is not able to deal with occlusion problems or presence of strongly cluttered background. Therefore the integration of prior shape knowledge about the objects in the segmentation task represents a natural way to solve occlusion problems and can be considered as a third generation of active contours. As we will see, we propose a model that exploits the advantages of the three generations of active contours.

The shape prior can be defined by different models such as Fourier descriptors, medial axis or atlas-based parametric models. A performant shape representation has to capture all natural variations, be invariant with respect to spatial transformations and compact to reduce the number of model parameters. A solution consists in using a set of training shapes of object of interest and look for a compact representation which can best represent the training set. Shape models based on this idea are built on statistics such as the principal components analysis (PCA) [21, 22, 23, 24]. Recently, the level set representation of shapes has been employed as a shape model [22, 23, 24]. This shape description presents strong advantages since parametrization free, it can represent shapes of any dimension such as curves, surfaces and hyper-surfaces and basic geometric properties such as the curvature and the normal to contours are easily deduced. Finally, this shape representation is also naturally consistent with the level set framework of active contours.

The integration of a geometric shape model in the segmentation process can be done by a shape registration method to map the prior shape onto the snake shape (the target shape) as done in [22, 25, 23]. The shape registration problem consists in determining a geometric deformation field (rigid, affine, non-rigid) between a reference shape and a target shape that optimizes a shape correspondance criterion. In [22], Leventon *et al.* have used a level set representation of the prior shape and the active contours and they have registered both shapes by maximizing a similarity measure between the two level sets. They have observed that the level set representation improves the registration, both in terms of robustness and accuracy. The main reason is that the contour point-wise correspondance problem (landmarks correspondance problem) is replaced by a grid point-wise intensity correspondance problem between the shape prior and snake surfaces that is easier to solve.

This paper aims at proposing a method to segment structures of interest whose global shape is given. For the

reasons previously described, we will use a level set representation of shapes and employ a compact model to represent shapes of a training set. The model developed by Leventon *et al.* in [22], based on the principal components analysis of training shapes represented by level set functions, appears to fulfil our shape model conditions. Indeed, this model allows us to represent *global shape variations* of a training family of a structure of interest. This shape information being global, it does not enable us to precisely capture all local shape variations present in the training set. However, we think that local shape variations of the object to segment can be accurately and efficiently segmented by boundary-based active contours. Combining a shape prior (not probabilistic) with the geometric/geodesic active contours, Chen *et al.* have proposed in [25] a variational model that simultaneously achieves registration and segmentation. Therefore, we firstly propose to extend the segmentation model of Chen *et al.* by integrating the statistical shape model of Leventon *et al.*. We then add a region-based energy term based on the Mumford-Shah functional [9] to improve the robustness of our segmentation model with respect to (w.r.t.) noise, poor image contrast and initial position of the contour. We will also prove the existence of a solution for our variational segmentation problem.
In section 2, we briefly review some state-of-the-art results that are directly connected to our work. In section 3, we define our new variational model to address the object segmentation problem with a prior shape knowledge and we derive the system of evolution equations minimizing the proposed energy. Then in section 4, we introduce the Mumford-Shah functional in our framework. We present experimental results to validate the proposed method on 2-D synthetic and medical images. We discuss our segmentation model and compare it with other ones in Section 5 and conclude in Section 6. Finally, we prove in appendix the existence of a minimizer for our variational segmentation model.

2. ACTIVE CONTOUR FAMILIES AND PCA SHAPE MODELING

In this section, we propose to briefly review the three main families of active contours, i.e. the boundary-based, the region-based and the shape-based active contours. We also present the shape model of Leventon *et al.* [22].

2.1. Boundary-Based/Geodesic Active Contours

The first model of boundary-based active contour was proposed by Kass *et al.* [10]. This model locates sharp image intensity variations by deforming a curve C towards the edges of objects. The evolution equation of C is given by the minimization of the energy functional $F(C) = \int_0^1 |C'(p)|^2 dp + \beta \int_0^1 |C''(p)|^2 dp + \lambda \int_0^1 g^2(|\nabla I(C(p))|) dp$ which g is an edge detecting function vanishing at infinity. This segmentation model presents two main drawbacks. Firstly, the functional F depends on the parametrization of the curve C. This means that different parametrizations of the curve may give different solutions for the same initial condition. Secondly, this approach does not take into account changes of topology. As a result, the final curve has the same topology as the initial one. To overcome the first limitation, Caselles *et al.* [26] and Kichenassamy *et al.* [27, 28] have proposed a new energy functional which is invariant w.r.t. a new curve parametrization. The new intrinsic energy functional is $F^{GAC}(C) = 2\sqrt{\lambda} \int_0^{L(C)} g(|\nabla I(C(s))|) ds$, where ds is the Euclidean element of length. F^{GAC} is actually a new length obtained by weighting the Euclidean element of length by the function g which contains information regarding the objects boundaries. Caselles *et al.* have also proved in [26] that the final curve is a geodesic in a Riemannian space. This geodesic is computed by the calculus of variations providing the Euler-Lagrange equations of F^{GAC} and the gradient descent method which gives the flow minimizing the functional F^{GAC}: $\partial_t C = (\kappa g - < \nabla g, \mathcal{N} >)\mathcal{N}$, where $\mathcal{N}$ is the unit normal to the curve C and κ is its curvature. To overcome the second limitation, Osher and Sethian proposed the level set method in [11, 5, 8]. The curve C is thus implicitely represented by a level set function φ. Finally, a curve evolution $\partial_t C = F\mathcal{N}$ can be re-written in a level set formulation: $\partial_t \varphi = F|\nabla \varphi|$ which evolution of the curve C coincides with the evolution of the zero level set of φ as shown in [26].

2.2. Region-Based Active Contours

Paragios and Deriche [15, 16] have employed new evolution criteria built from statistics on the regions to be segmented. Their variational method, called *geodesic active regions*, allows to unify boundary- and region-based statistical knowledge into a single energy functional which is minimized by a set of PDEs.
In [19, 20], a general paradigm for active contours is presented, derived from functionals that include local and

global statistical measures of homogeneity for the regions being segmented. Their criteria to minimize have the general form:

$$F^R(\Omega_{in}, \Omega_{out}, C) = \int_C k^b(x)ds + \int_{\Omega_{in}} k^{in}(x, \Omega_{in})d\Omega + \int_{\Omega_{out}} k^{out}(x, \Omega_{out})d\Omega, \quad (1)$$

where Ω^{in}, Ω^{out} are respectively the inner and the outer region of the active contour, k^{in} and k^{out} are the *descriptors* of these regions and k^b is the boundary descriptor. To determine the solution minimizing (1), shape optimization tools [29, 30] are needed to differentiate (1) w.r.t. the domains Ω_{in} and Ω_{out} that evolve in time. Then, the evolution equations of active contours are deduced from the derivative of F^R to minimize as fast as possible F^R. By using the entropy descriptor from [19], the following flow produces very good segmentation results as we can see on Figure 2 (a) and (b).

In [17, 18, 31], a method to solve the Mumford-Shah functional [9] in the context of propagating contours is proposed. The Mumford and Shah's approach to solve the image segmentation problem has been extensively studied (see [4, 7] and [18] for references) but we restrict our attention to the active contours framework. The Mumford-Shah minimization problem is defined as follows:

$$\inf_{u,C} \{F^{MS}(u, C) = \int_\Omega |u - u_0|^2 dx + \mu \int_{\Omega - C} |\nabla u|^2 + \nu \mathcal{H}^{N-1}(C)\}, \quad (2)$$

where u corresponds to an optimal piecewise smooth approximation of an original image u_0, C represents the edges of u and the length of C is given by the (N-1)-dimensional Hausdorff measure $\mathcal{H}^{N-1}(C)$ [2]. Chan and Vese [17, 18] have proposed a model to minimize the functional (2). A piecewise smooth approximation of a given image is computed (which enables image denoising) by minimizing the following functional w.r.t. a level set function φ and two functions u_{in} and u_{out} (we consider here only two regions Ω_{in} and Ω_{out} even if Chan and Vese have solved the complete image partitionning problem):

$$F^{MS}_{CV}(u_{in}, u_{out}, \varphi) = \nu \int_\Omega |\nabla H(\varphi)| + \int_\Omega (|u_{in} - u_0|^2 + \mu |\nabla u_{in}|^2) H(\varphi) dx + \int_\Omega (|u_{out} - u_0|^2 + \mu |\nabla u_{out}|^2) H(-\varphi) dx, \quad (3)$$

where H is the Heaviside function. The evolution equation of the level set function embedding the active contour is as follows:

$$\partial_t \varphi = \delta(\varphi)(\nu\kappa + |u_{out} - u_0|^2 + \mu |\nabla u_{out}|^2 - |u_{in} - u_0|^2 - \mu |\nabla u_{in}|^2). \quad (4)$$

An example of segmentation using this model is given on Figure 2 (c)-(e).

2.3. Shape-Based Active Contours

In [22, 32], Leventon *et al.* have developed active contours that use a statistical shape model defined by a PCA. In their approach, the active contour evolves locally based on image gradients and curvature and globally towards the maximum a posteriori (MAP) probability of position and shape of the prior shape model. However, this a posteriori probability is maximized at each iteration by an independant optimization process, which means that the final evolution equation is not a PDE since two independant stages are necessary to evolve the surface. The evolution equation is the following:

$$u(t+1) = u(t) + \lambda_1 \left(g(c + \kappa)|\nabla u(t)| + \langle \nabla u(t), \nabla g \rangle\right) + \lambda_2 (u^\star(t) - u(t)), \quad (5)$$

where $u^\star$ is the shape prior. The second term of the right-hand side of (5) weighted by λ_1 represents the classical term of the geodesic active contour. And the third term depending on λ_2 drives the shape of the active contour

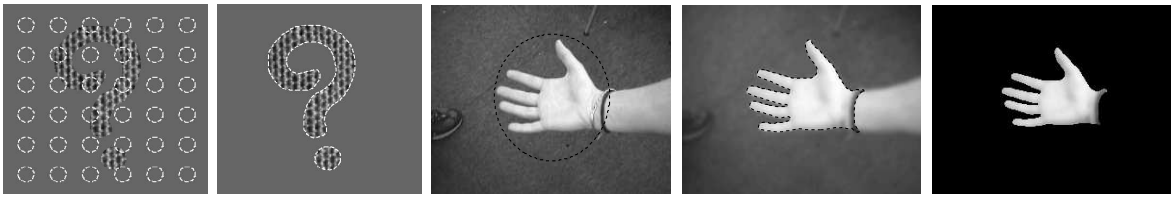

(a) (b) (c) (d) (e)

Fig. 2. Figures (a),(b) show a segmentation using the region-based active contour of Jehan-Besson *et al.*, Figures (c),(d) present a segmentation using the active contour of Chan and Vese based on the Mumford-Shah functional and Figure (e) represents a smooth approximation of the hand.

towards the shape prior given by the MAP estimation.
In [33], Tsai *et al.* have integrated the previous shape model of Leventon *et al.* in the piecewise-constant version of the Mumford-Shah functional proposed by Chan and Vese in [17] to segment images containing known object types.
In [34, 25], Chen *et al.* have designed a novel variational model that incorporates prior shape knowledge into geometric/geodesic active contours. On the contrary to Leventon's approach, the shape model $C^\star$ of Chen is not a probabilistic one. It is computed as the average of a training set of rigidly aligned curves. However, this variational approach proves the existence of a solution minimizing their energy functional, which is not the case in the Leventon's method. Chen's functional is defined as:

$$F^C(C,\mu,\theta,T) = \int_0^1 \left(g(|\nabla I(C(p))|) + \frac{\lambda}{2} d^2(\mu R C(p) + T)\right) |C'(p)| dp, \tag{6}$$

where C is the active contour, (μ,θ,T) are the parameters of a rigid transformation (scale, orientation and translation) and d is the distance to $C^\star$, the target shape. This functional is thus minimized when the active contour has captured both high image gradients and the shape prior. They have showed the good ability of the model to extract real-world structures in which the complete boundary was either missing or had low resolution and contrast [34, 25].
In [23, 35], Paragios *et al.* have built a new level set representation of shape from a training set in order to capture both global and local shape variations. They have used it to non-rigidly register two shapes and to segment objects with a modified version of the geodesic active regions defined in [15, 16].
In [36, 37, 38], Cremers *et al.* have modified the Mumford-Shah functional to incorporate two statistical models of parametric shape in order to efficiently segment known objects in presence of misleading information due to noise, occlusion and strongly cluttered background. Concerning the shape model, they have used a multivariate Gaussian distribution in [36] and a nonlinear shape statistic derived from an extension of the kernel PCA in [37].

2.4. The Statistical Shape Model of Leventon et al.

2.4.1. Definition

We finish this section by presenting the shape model developed by Leventon *et al.* [22] which we use in our segmentation model. This shape model is based on the PCA that aims at capturing the main variations of a training set while removing redundant information. In [21], Cootes and Taylor have used this technique on parametric contours to segment different kind of objects. The new idea introduced by Leventon *et al.* [22] is to apply the PCA not on the parametric geometric contours but on the signed distance functions (SDFs) of these contours which are implicit and parameter free representations. They justified this choice in two ways. Firstly, SDFs provide a *stronger* tolerance than the parametric curves to slight misalignments during the alignment process of the training data since *the values of neighboring pixels are highly correlated in a SDF*. Secondly, this intrinsic contour representation also improves the shape registration process in terms of robustness, accuracy and speed.

Indeed, the problem of the point-wise correspondence of contours (landmarks correspondance) is replaced by a problem of intensity correspondence on grid points which is easier to solve.
From a geometric point of view, the PCA analysis determines the best orthonormal basis $\{\mathbf{e}_1...\mathbf{e}_m\}$ of $\mathbf{R}^m$ to represent a set of n points $\{\phi_1...\phi_n\}$ in the sense of the least squares fitting. Vectors $\{\mathbf{e}_i\}$ are given by the eigenvectors of the covariance matrix $\mathbf{\Sigma} = \frac{1}{n}MM^\top$ where M is a matrix whose column vectors are the n aligned training SDFs $\{\phi_j\}$. Vectors $\{\mathbf{e}_i\}$ correspond to the principal variation directions of the set of n points. They are called the *principal components*. Moreover, the first p principal axes define a reduced p-dimensional vector space in $\mathbf{R}^m$ equivalent to a hyper-plane minimizing the sum of squared distances between this hyper-plane and the set of n points. It is important to note that the accuracy of the fitting of this p-D hyper-plane in relation to the set of points can be measured in percentage by the formula $\beta = \sum_{k=1}^{p}\lambda_k / \sum_{k=1}^{n}\lambda_k$ where λ_k are the eigenvalues of $\mathbf{\Sigma}$. Thus, it is possible to arbitrarly fix the fitting percentage β and represent the data in a sub-vector space of dimension p. In practice, only the first principal modes are necessary to model the biggest variations present in our training set. These p principal components are sorted in a matrix $\mathbf{W}_p$. Thus, the projected data $\hat{\phi}$ in the p-D space of a training data ϕ in $\mathbf{R}^m$ is given by:

$$\hat{\phi} = \overline{\phi} + \mathbf{W}_p\mathbf{x}_{pca}, \tag{7}$$

where $\mathbf{x}_{pca}$ is the vector of eigencoefficients:

$$\mathbf{x}_{pca} = \mathbf{W}_p^\top(\phi - \overline{\phi}). \tag{8}$$

If we suppose that the probability density funtion (PDF) of the training set is Gaussian then the probability of $\hat{\phi}(\mathbf{x}_{pca})$ is

$$P(\hat{\phi}(\mathbf{x}_{pca})) = \frac{1}{(2\pi)^{p/2}|\mathbf{\Lambda}_p|^{1/2}} exp(-\frac{1}{2}\mathbf{x}_{pca}^\top\mathbf{\Lambda}_p^{-1}\mathbf{x}_{pca}), \tag{9}$$

where $\mathbf{\Lambda}_p$ is a diagonal matrix containing the first p eigenvalues.

2.4.2. Implementation

The first stage consists in aligning rigidly the training curves representing the object of interest. This is realized using the shape similarity measure introduced by Chen *et al.* [34, 25]:

$$a(C_1, C_j^{new}) = \text{aera of } (A_1 \cup A_j^{new} - A_1 \cap A_j^{new}) \quad \text{for } 2 \leq j \leq n, \tag{10}$$

where A_1 and A_j^{new} denote respectively the interior regions of the curves C_1 and C_j^{new} where C_j^{new} is the resulting curve from the rigid registration such that $C_j^{new} = s_j R_{\theta_j} C_j + T_j$ and n is the number of training curves. C_1 and C_j are aligned when the measure a is minimized for the appropriate values $s_j^\star$, $\theta_j^\star$ and $T_j^\star$. These values are obtained by a global optimization algorithm called the genetic algorithm [39].
The second stage of the PCA consists in doing the singular values decomposition on the SDFs of the aligned training curves using the code provided by Numerical Recipies [40] on the matrix $\mathbf{\Sigma}^{dual} = \frac{1}{n}M^\top M$ to extract the n eigenvalues $\mathbf{e}_{pca}^{i,dual}$ and the eigenvectors $\lambda_{pca}^{i,dual}$. Note that the PCA is performed on $\mathbf{\Sigma}^{dual}$ rather than $\mathbf{\Sigma}$ to give faster and more accurate results. The eigenvectors $\mathbf{e}_{pca}^i$ and the eigenvalues λ_{pca}^i are then given by $\mathbf{e}_{pca}^i = M\mathbf{e}_{pca}^{i,dual}$ and $\lambda_{pca}^i = \lambda_{pca}^{i,dual}$.

2.4.3. Examples

In this paper, we have considered two sets of 2-D shapes of interest: one containing ellipses and the other one left brain ventricles. For the ellipse, we have generated a training set of 30 ellipses by changing the size of a principal axis with a Gaussian probability function and applied the PCA on the SDFs of 30 training ellipses. We have obtained one principal component that fits at 98% the set of ellipses. Figure 3 shows the aligned training ellipses and the shape function corresponding to the mean and the eigenmode of variation of the training set.
For the left brain ventricle, we have employed 2-D medical images. We have extracted 45 2-D images of left

(a)

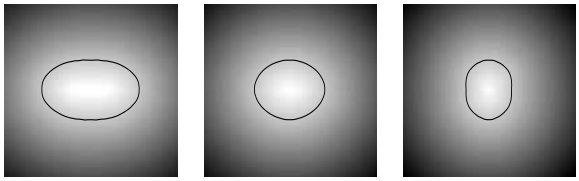

(b) -2λ (c) Mean (d) 2λ

Fig. 3. Figure (a) presents the 30 aligned training ellipses with the mean ellipse in dotted line. Figure (c) shows the mean value $\overline{\phi}$. Figures (b) and (d) present $\overline{\phi} \pm 2\lambda_1 \mathbf{e}_1$, the unique eigenmode of variation of SDF ellipses whose λ_1 is the eigenvalue. The zero level sets of the shape function $\hat{\phi}$ is plotted in solid dark line.

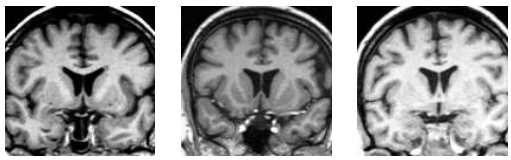

Fig. 4. Three T1-Weighted Magnetic Resonance images of brain.

ventricles from several coronal slices of T1-Weighted Magnetic Resonance images (MRI) of healthy voluntaries (Figure 4) to build our statistical shape model. We have applied the PCA and obtained three principal components that fit at 88.2% the set of 45 SDFs of ventricles. Figure 5 shows the aligned training ventricles and the shape function corresponding to the mean and the three main eigenmodes of variation of the training set.

3. OUR OBJECT SEGMENTATION MODEL

3.1. The Proposed Segmentation Model

We propose the following energy functional to address the problem of object segmentation using a geometric shape prior and local image information:

$$F_1 = \beta_b F_{boundary}(C) + \beta_s F_{shape}(C, \mathbf{x}_{pca}, \mathbf{x}_T), \tag{11}$$

$$\text{where } F_{boundary} = \oint_0^1 g(|\nabla I(C(q))|)|C'(q)|dq, \tag{12}$$

$$F_{shape} = \oint_0^1 \hat{\phi}^2(\mathbf{x}_{pca}, h_{\mathbf{x}_T}(C(q)))|C'(q)|dq. \tag{13}$$

where C is the active contour, $\hat{\phi}$ is the shape function of the object of interest given by the PCA (see Equation (7)), $\mathbf{x}_{pca}$ is the vector of PCA eigencoefficients, $h_{\mathbf{x}_T}$ is an element of a group of geometric transformations parametrized

(a)

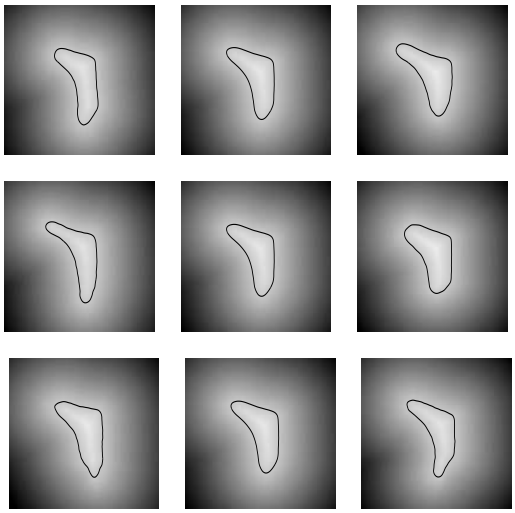

Fig. 5. Figure (a) presents the 45 aligned training ventricles with the mean left ventricle in dotted line. On Figure (i), the middle column is the mean value and each row presents an eigenmode of variation of ventricles. The zero level sets of the shape function $\hat{\phi}$ is plotted in solid dark line.

by $\mathbf{x}_T$ (the vector of parameters), g is an edge detecting function and β_b, β_s are arbitrary positive constants that balance the contributions of the boundary, shape and region terms.
The proposed functional F_1 is an extension of the work of Chen *et al* [34, 25] where we have integrated the statistical shape model of Leventon *et al* [22]. In the following section, we will analyse the shape term.

3.2. The Shape Term F_{shape}

F_{shape} is a functional introduced by the authors in [41] that depends on the active contour C, the vector $\mathbf{x}_{pca}$ of PCA eigencoefficients and the vector $\mathbf{x}_T$ of geometric transformations. This functional evaluates the shape difference between the contour C and the zero level set $\hat{C}$ of the shape function $\hat{\phi}$ provided by the PCA. It is an extension of the shape-based term of Chen *et al* [34, 25] coupled with the statistical shape model of Leventon *et al* [22]. To give an interpretation of F_{shape}, let us take a rigid transformation with the scale parameter equal to one, the angle and the vector of translations equal to zero, Thus, the function $\hat{\phi}^2$ at the point $C(q)$ is:

$$\begin{aligned}\hat{\phi}^2(\mathbf{x}_{pca}, h_{\mathbf{x}_T}(C(q))) = \hat{\phi}^2(\mathbf{x}_{pca}, C(q)) \simeq \\ \| \hat{C}_{\mathbf{x}_{pca}}(p_{min}) - C(q) \|^2,\end{aligned} \tag{14}$$

where $\| \, . \, \|$ stands for the Euclidean norm.
The equality is not strict since the shape function $\hat{\phi}$ is not a SDF as Leventon noticed in [22, 32]. However, the PCA applied on aligned SDFs of a training set produces shape functions *very close* to SDFs. The case of a strict equality in Equation (14), i.e. the case of $\hat{\phi}$ is a true SDF, will be discussed in Section 5. Figure 6 illustrates the

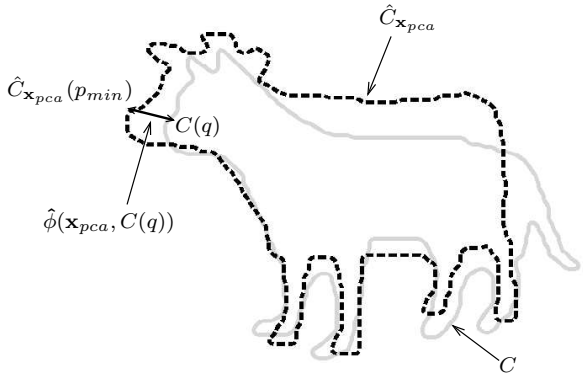

Fig. 6. Illustration of the function $\hat{\phi}(\mathbf{x}_{pca}, C(q))$: the square shape function is approximatively equal to the square Euclidean distance between the point $C(q)$ and the closest point $\hat{C}_{\mathbf{x}_{pca}}(p_{min})$ on the zero level set $\hat{C}_{\mathbf{x}_{pca}}$ of $\hat{\phi}(\mathbf{x}_{pca})$.

function $\hat{\phi}$.
Finally, F_{shape} is obtained by integrating $\hat{\phi}^2$ along the active contour, which defines the shape similarity measure equivalent to the sum of square differences (SSD).
The minimization of F_{shape} allows us to increase the similarity between the active contour and the shape model. The functional is minimized using the calculus of variations and the gradient descent method which provide three flows acting on the curve C, the vector of eigencoefficients $\mathbf{x}_{pca}$ and the vector of geometric transformations $\mathbf{x}_T$.
We analyse each of the three flows by fixing the two others. The flow minimizing F_{shape} w.r.t. the curve C is the classical geometric/geodesic flow [28, 26]:

$$\left\{ \begin{array}{l} \partial_t C(t,q) = \\ \quad (\hat{\phi}^2 \kappa - < \nabla \hat{\phi}^2, \mathcal{N} >) \mathcal{N} \text{ in }]0, \infty[\times [0,1], \\ C(0,q) = C_0(q) \text{ in } [0,1]. \end{array} \right. \tag{15}$$

The PDE defined in Equation (15) changes the active contour shape into any shape provided by the PCA model. This shape morphing has two main advantages. First, it is independant of the contour parametrization because of the intrinsic level set representation. This means that the landmarks correspondence problem is replaced by a grid point-wise intensity correspondence which is easier to solve. Then, it is more accurate than parametrized shape morphing since the degree of deformation of level set functions is higher. Figure 7 presents the morphing between two curves.
The flow minimizing F_{shape} w.r.t. the vector of eigencoefficients $\mathbf{x}_{pca}$ is:

$$\left\{ \begin{array}{l} d_t \mathbf{x}_{pca}(t) = -2 \int_0^1 \hat{\phi} \nabla_{\mathbf{x}_{pca}} \hat{\phi} \, |C'| dq \text{ in }]0, \infty[\times \Omega_{pca}, \\ \mathbf{x}_{pca}(t=0) = \mathbf{x}_{pca_0} \text{ in } \Omega_{pca}. \end{array} \right. \tag{16}$$

$$\text{with} \quad \nabla_{\mathbf{x}_{pca}} \hat{\phi} = \begin{pmatrix} \mathbf{e}^1_{pca} \\ \vdots \\ \mathbf{e}^p_{pca} \end{pmatrix}, \tag{17}$$

where $\mathbf{e}^i_{pca}$ is the ith principal component/eigenvector of the PCA presented in Section 2.4 and Ω_{pca} is the space of PCA variables defined by $\Omega_{pca} = [-3\lambda_1, 3\lambda_1] \times ... \times [-3\lambda_p, 3\lambda_p]$ whose λ_i is the eigenvalue of the ith principal component. The evolution Equation (16) changes the shape function $\hat{\phi}$ to match its zero level set with the active contour. Figure 8 presents this shape matching.

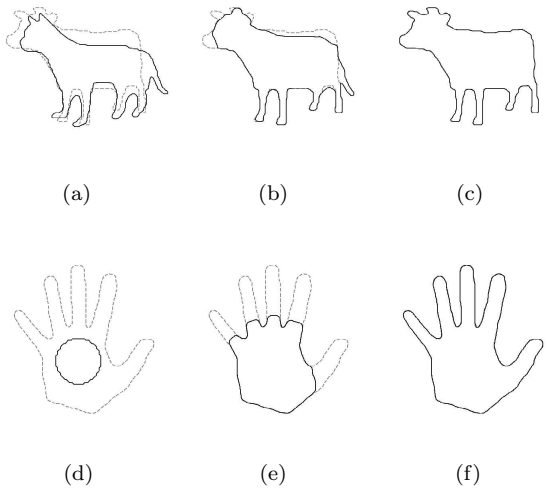

Fig. 7. Minimization of F_{shape} with the flow given in Equation (15), $\mathbf{x}_T$ and $\mathbf{x}_{pca}$ being fixed. Active contour is in solid line and the shape prior in dotted line. Figures (a)-(c) show the matching of a cat (initial active contour) into a cow (shape prior). Figures (d)-(f) present the matching of a circle into a hand.

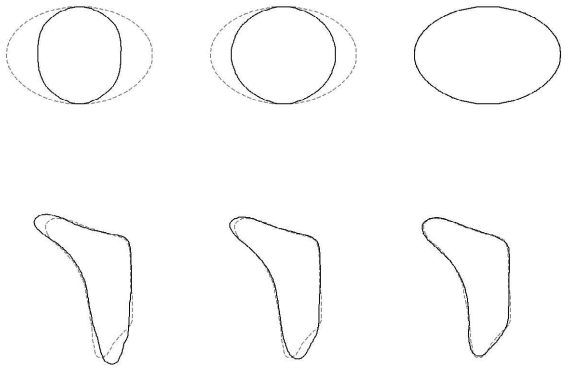

Fig. 8. Minimization of F_{shape} with the flow given in Equation (16), ϕ and $\mathbf{x}_T$ being fixed. The prior shape is in solid line and the active contour in dotted line. The first row presents the shape evolution of the PCA model of 30 ellipses (see Section 2.4.3). The zero level set of the shape function $\hat{\phi}$ evolves to match with the active contour representing an ellipse taken in the training set. The second row shows the shape evolution of the PCA model of 45 left brain ventricles (see also Section 2.4.3). The shape model changes to match with the active contour representing a left brain ventricle taken in the training set.

And the flow minimizing F_{shape} w.r.t. the vector of geometric transformations $\mathbf{x}_T$ is:

$$\left\{ \begin{array}{l} d_t \mathbf{x}_T(t) = \\ \quad -2 \int_0^1 \hat{\phi} < \nabla \hat{\phi}, \nabla_{\mathbf{x}_T} h_{\mathbf{x}_T}(C) > |C'| dp \text{ in }]0, \infty[\times \Omega_T, \\ \mathbf{x}_T(t=0) = \mathbf{x}_{T_0} \text{ in } \Omega_T. \end{array} \right. \tag{18}$$

In (15), (16) and (18), the function $\hat{\phi}$ is evaluated at $(\mathbf{x}_{pca}, h_{\mathbf{x}_T}(C(q))$. In our work, we have considered the rigid (denoted by $h_{\mathbf{x}_T^r}$) and the affine (denoted by $h_{\mathbf{x}_T^a}$) transformations:

$$h_{\mathbf{x}_T^r} : x \rightarrow h_{(s,\theta,T)}(x) = sR_\theta x + T, \tag{19}$$

$$h_{\mathbf{x}_T^a} : x \rightarrow h_{(s_x,s_y,\theta,s_h,T)}(x) = R_{sc}R_\theta R_{sh}x + T, \tag{20}$$

where

$$R_{sc} = \begin{pmatrix} s_x & 0 \\ 0 & s_y \end{pmatrix}, R_\theta = \begin{pmatrix} \cos\theta & \sin\theta \\ -\sin\theta & \cos\theta \end{pmatrix},$$
$$R_{sh} = \begin{pmatrix} 1 & s_h \\ 0 & 1 \end{pmatrix} \text{ and } T = \begin{pmatrix} T_x \\ T_y \end{pmatrix}. \tag{21}$$

The vector of rigid transformations $\mathbf{x}_T^r$ is composed of a scale parameter s, an angle of rotation θ and a vector of translations T and the vector of affine transformations $\mathbf{x}_T^a$ is composed of two scale parameters s_x in x-direction and s_y in y-direction, an angle of rotation θ, a shearing parameter s_h and a vector of translations T. Finally, the domain of the rigid/affine transformations is called Ω_T.
As a consequence, the gradient term $\nabla_{\mathbf{x}_T} h_{\mathbf{x}_T}$ in (18) depending on geometric transformations is:

$$\nabla_{\mathbf{x}_T^r} h_{\mathbf{x}_T^r}(x) = \begin{pmatrix} \frac{\partial h_{\mathbf{x}_T^r}}{\partial s}(x) = R_\theta x \\ \frac{\partial h_{\mathbf{x}_T^r}}{\partial \theta}(x) = s\partial_\theta R_\theta x \\ \frac{\partial h_{\mathbf{x}_T^r}}{\partial T}(x) = \mathbf{1} \end{pmatrix}, \tag{22}$$

for 2-D rigid transformations and

$$\nabla_{\mathbf{x}_T^a} h_{\mathbf{x}_T^a}(x) = \begin{pmatrix} \frac{\partial h_{\mathbf{x}_T^a}}{\partial s_x}(x) = (\partial_{s_x} R_{sc})R_\theta R_{sh}x \\ \frac{\partial h_{\mathbf{x}_T^a}}{\partial s_y}(x) = (\partial_{s_y} R_{sc})R_\theta R_{sh}x \\ \frac{\partial h_{\mathbf{x}_T^a}}{\partial \theta}(x) = R_{sc}(\partial_\theta R_\theta)R_{sh}x \\ \frac{\partial h_{\mathbf{x}_T^a}}{\partial s_h}(x) = R_{sc}R_\theta(\partial_{s_h} R_{sh})x \\ \frac{\partial h_{\mathbf{x}_T^a}}{\partial T}(x) = \mathbf{1} \end{pmatrix}, \tag{23}$$

for 2-D affine transformations. The evolution equation (18) realizes the rigid and affine registration between the zero level set of the shape model $\hat{\phi}$ and the active contour. Figures 9 and 10 present affine registrations.

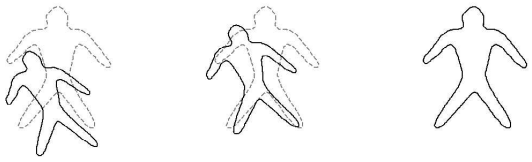

Fig. 9. Minimization of F_{shape} with the flow given in Equation (18), ϕ and $\mathbf{x}_{pca}$ being fixed. The row of images represents the affine registration of a prior shape in solid line into an active contour in dotted line.

Note that the function $\hat{\phi}$ is evaluated at $(\mathbf{x}_{pca}, h_{\mathbf{x}_T}(C(q))$ in Equations (15-18).
Let us now express the previous equations in a variational level set formulation as presented in [42, 25]. The level set approach of [42], rather than [28, 26], will be used to prove the existence of solution minimizing our energy functional in the space of functions with bounded variation. The level set formulation of the shape functional from Equation (13) is:

$$F_{shape} = \int_\Omega \hat{\phi}^2(\mathbf{x}_{pca}, h_{\mathbf{x}_T}(x))|\nabla\varphi|\delta(\varphi)d\Omega, \tag{24}$$

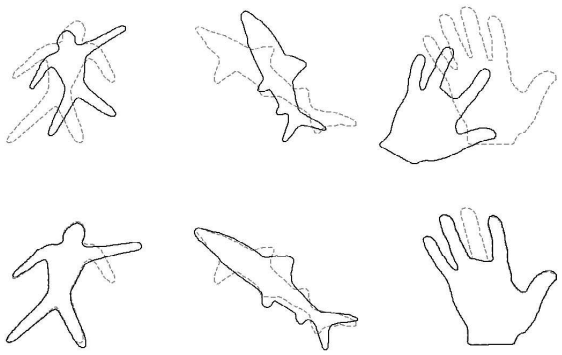

Fig. 10. Minimization of F_{shape} with the flow given in Equation (18), ϕ and $\mathbf{x}_{pca}$ being fixed. Each column presents the affine registration of a prior shape in solid line into an active contour in dotted line. The first row shows the initial position of the shapes and the second row the registered shapes. This registration process works with shapes having different local structures and missing information.

where φ is a level set function embedding the active contour C, $\delta(.)$ is the Dirac function and $\delta(\varphi)$ is the contour measure on $\{\varphi = 0\}$. And the level set formulation of Equations (15-18) are:

$$\begin{cases} \partial_t \varphi(t,x) = \left(\hat{\phi}^2 \kappa - \langle \nabla \hat{\phi}^2, \frac{\nabla \varphi}{|\nabla \varphi|} \rangle\right) \delta(\varphi) \\ \qquad\qquad \text{in }]0,\infty[\times\Omega, \\ \varphi(0,x) = \varphi_0(x) \text{ in } \Omega, \\ \frac{\delta(\varphi)}{|\nabla \varphi|} \partial_{\mathcal{N}} \varphi = 0 \text{ on } \partial\Omega, \end{cases} \tag{25}$$

$$\begin{cases} d_t \mathbf{x}_{pca}(t) = -2 \int_\Omega \hat{\phi} \nabla_{\mathbf{x}_{pca}} \hat{\phi} |\nabla \varphi| \delta(\varphi) d\Omega \\ \qquad\qquad \text{in }]0,\infty[\times\Omega_{pca}, \\ \mathbf{x}_{pca}(t=0) = \mathbf{x}_{pca_0} \text{ in } \Omega_{pca}, \end{cases} \tag{26}$$

$$\begin{cases} d_t \mathbf{x}_T(t) = \\ \qquad -2 \int_\Omega \hat{\phi} \langle \nabla \hat{\phi}, \nabla_{\mathbf{x}_T} h_{\mathbf{x}_T} \rangle |\nabla \varphi| \delta(\varphi) d\Omega \\ \qquad\quad \text{in }]0,\infty[\times\Omega_T, \\ \mathbf{x}_T(t=0) = \mathbf{x}_{T_0} \text{ in } \Omega_T. \end{cases} \tag{27}$$

In our segmentation model, the flows given by the Equations (25-27) are simultaneously used to constraint the active contour to get a shape of interest whatever the position of the active contour in the image.
In a nutshell, we have defined in this section a process to force the active contour to get a particular shape. In the next section, we will introduce image information in our segmentation method to capture the object of interest in the image.

3.3. Evolution Equations Minimizing The Functional F_1

In this section, we compute the system of coupled evolution equations that minimizes the functional (11) in order to realize the object segmentation with a prior shape and local image information. We directly write the system of flows in the Eulerian/level set formulation. We define the function

$$\begin{aligned} &f(x, \mathbf{x}_{pca}, \mathbf{x}_T) = \\ &\quad \beta_b g(|\nabla I(x)|) + \beta_s \hat{\phi}^2(\mathbf{x}_{pca}, h_{\mathbf{x}_T}(x)), \end{aligned} \tag{28}$$

such that

$$F_1 \quad = \quad \int_\Omega f(x, \mathbf{x}_{pca}, \mathbf{x}_T)|\nabla\varphi|\delta(\varphi)d\Omega. \tag{29}$$

The system of flows minimizing F_1 is thus

$$\begin{cases} \partial_t\varphi(t,x) = \\ \quad \left(f\kappa - \langle\nabla f, \frac{\nabla\varphi}{|\nabla\varphi|}\rangle\right)\delta(\varphi) \text{ in }]0,\infty[\times\Omega, \\ \varphi(0,x) = \varphi_0(x) \text{ in } \Omega, \\ \frac{\delta(\varphi)}{|\nabla\varphi|}\partial_{\mathcal{N}}\varphi = 0 \text{ on } \partial\Omega. \end{cases} \tag{30}$$

$$\begin{cases} d_t\mathbf{x}_{pca}(t) = \\ \quad -2\beta_s\int_\Omega \hat{\phi}\nabla_{\mathbf{x}_{pca}}\hat{\phi}|\nabla\varphi|\delta(\varphi)d\Omega \text{ in } \Omega_{pca}, \\ \mathbf{x}_{pca}(t=0) = \mathbf{x}_{pca_0} \text{ in } \Omega_{pca}. \end{cases} \tag{31}$$

$$\begin{cases} d_t\mathbf{x}_T(t) = \\ \quad -2\beta_s\int_\Omega \hat{\phi} < \nabla\hat{\phi}, \nabla_{\mathbf{x}_T}h_{\mathbf{x}_T} > |\nabla\varphi|\delta(\varphi)d\Omega \text{ in } \Omega_T, \\ \mathbf{x}_T(t=0) = \mathbf{x}_{T_0} \text{ in } \Omega_T. \end{cases} \tag{32}$$

3.4. Implementation issues

The evolution equations (40) to (42) are numerically solved by iterating the following stages until convergence is reached:

1. Computation of the shape function $\hat{\phi}(\mathbf{x}_{pca}, \mathbf{x}_T)$ using Equation (7) and performing the rigid and affine transformations (scaling, rotation, translations and shearing) with the B-splines interpolation method [43].

2. Calculation of the gradient $\nabla\hat{\phi}$ using a central difference sheme. The term $\nabla_{\mathbf{x}_{pca}}\hat{\phi}$ is given by the eigenvectors of the PCA model and $\nabla_{\mathbf{x}_T}h_{\mathbf{x}_T}$ is computed according to Equations (22) and (23).

3. Discretization of terms $|\nabla\varphi|$ and $\langle\nabla f, \frac{\nabla\varphi}{|\nabla\varphi|}\rangle$ with the Osher-Sethian numerical scheme [11]. Computation of the curvature with central difference schemes. The Dirac function δ and the Heaviside function H are computed by slightly regularized versions following [42, 25].

4. Calculation of the temporal derivative using a forward difference approximation.

5. Redistancing the level set function at every iteration with the Fast Marching Method of Adalsteinsson and Sethian [44].

3.5. Experimental Results

3.5.1. Synthetic Images

In the first experiment, we have used our segmentation model to extract an ellipse which is partially cut. Figure 11 presents a geodesic active contour *without* a shape prior and Figure 12 *with* a shape prior by taking $\beta_s = 1/3$, $\beta_b = 1$ and $\Delta t = 0.4$. We can see on figure 12 that the active contour has captured high image gradients and also the missing part thanks to the information contained in the prior shape model.
In the second experiment, our extraction model is applied to segment an ellipse with irregular boundaries which is partially occluded by a vertical bar. Figure 13 presents the geodesic active contour *without* a shape prior and Figure 14 *with* a shape prior by choosing $\beta_s = 1/3$, $\beta_b = 1$ and $\Delta t = 0.4$.
Thus, our shape-based active contour model can segment objects with missing information, occlusion and local shape variations.

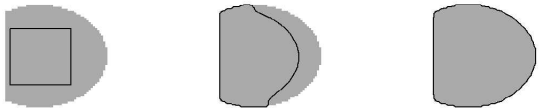

Fig. 11. Evolution of a geodesic active contour *without* a shape prior.

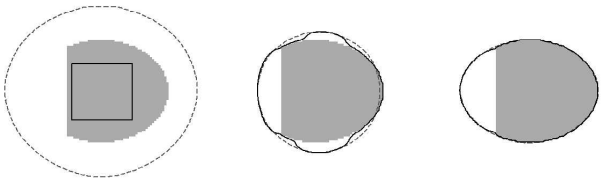

Fig. 12. Evolution of an active contour (in solid line) *with* a shape prior (in dotted line).

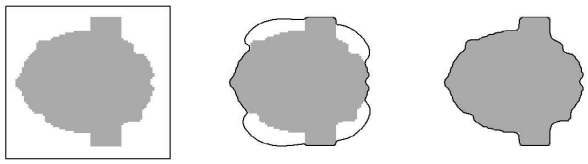

Fig. 13. Evolution of a geodesic active contour *without* a shape prior.

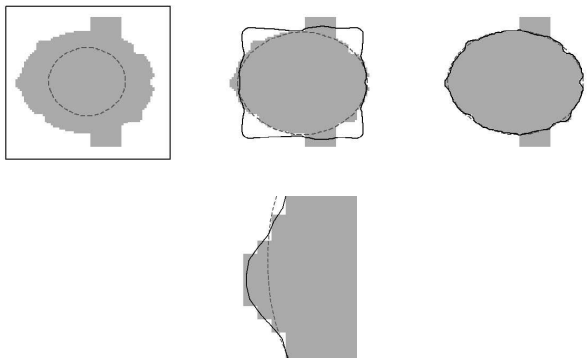

Fig. 14. The first row presents the evolution of an active contour (in solid line) *with* a shape prior (in dotted line). The second row is a zoom on the left point of the ellipse to show that the active contour is able to segment local structures even with the shape prior.

3.5.2. Medical Image

We have used our segmentation model to capture the left brain ventricle. Figure 15 presents the evolving geodesic active contour *without* a shape prior and Figure 16 *with* a shape prior by choosing $\beta_s = 2$, $\beta_b = 1$ and $\Delta t = 0.4$.

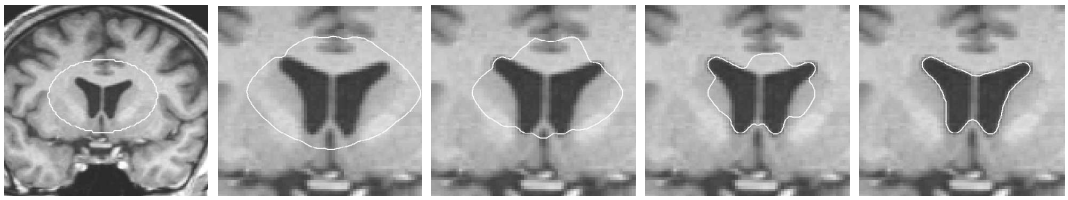

(a) (b) (c) (d) (e)

Fig. 15. Evolution of a geodesic active contour *without* a shape constraint.

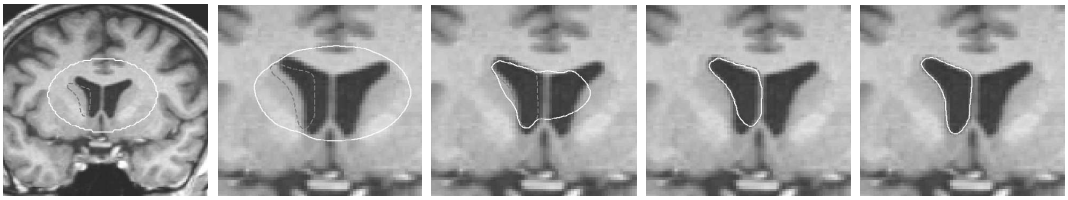

(a) (b) (c) (d) (e)

Fig. 16. Evolution of an active contour (in solid line) *with* a shape prior (in dotted line).

We observe on Figure 16 that the active contour has well captured the left ventricle whereas *the initial contour was around the two ventricles* (see Figure 16(a)). This segmentation result could not be obtained without a shape prior with the same initial contour as shown on Figure 15. The segmentation model has also provided the shape of the statistical model which best fits the ventricle lying in the image.

3.6. Using Other Segmentation Models

In the framework of variational models and PDEs, it is possible to use other segmentation models such as region-based segmentation methods developped in Section 2.2. The easiest way is to linearly combine energy functionals or PDEs directly. For examples, if we want to use the statistiscal measures of homogeneity introduced by Jehan-Besson *et al.* in [19], the new functional to be minimized will be $F^{new} = F_1(C, \mathbf{x}_{pca}, \mathbf{x}_T) + \lambda_R F^R(\Omega_{in}, \Omega_{out}, C)$ or if we want to use the Mumford-Shah approach of Chan and Vese [17, 18], the energy will be $F^{new} = F_1(C, \mathbf{x}_{pca}, \mathbf{x}_T) + \lambda_{MS} F^{MS}_{CV}(u_{in}, u_{out}, C)$. The PDE minimizing F^{new} will be a linear combination of the PDEs minimizing each term of F^{new}.
In the next section, we introduce a region homogeneity criterium into our segmentation model to improve its robustness.

4. REGION HOMOGENEITY FEATURES IN OUR SEGMENTATION MODEL

4.1. A Functional Based on the Mumford-Shah Model

In this section, we define a functional to drive the shape model towards a homogeneous intensity region with the shape of interest. If our objects of interest are supposed to have a smooth intensity surface then the Mumford-Shah (MS) model is the most adapted model to segment these objects.
At this stage, we had the choice to apply the MS model either on the active contour or the shape prior. Since the MS method applied on the active contour will extract globally homogeneous regions [18] and our objective is to capture an object belonging to a given shape space then the best solution is to apply the MS-based force on the shape prior. Indeed, this new force will globally drive the shape prior towards a homogeneous intensity region with the shape of interest. An illustration of this choice will appear in Section 4.4.

We have modified the Mumford-Shah functional (2) presented by Chan and Vese in [18] to segment a smooth region whose shape is described by the PCA model:

$$\begin{array}{c} F_{region}(\mathbf{x}_{pca}, \mathbf{x}_T, u_{in}, u_{out}) = \oint_{\hat{C}(\mathbf{x}_{pca}, \mathbf{x}_T)} ds + \\ \int_{\Omega_{in}(\mathbf{x}_{pca}, \mathbf{x}_T)} (|I - u_{in}|^2 + \mu |\nabla u_{in}|^2) d\Omega + \\ \int_{\Omega_{out}(\mathbf{x}_{pca}, \mathbf{x}_T)} (|I - u_{out}|^2 + \mu |\nabla u_{out}|^2) d\Omega, \end{array} \tag{33}$$

where the curve $\hat{C}$ is the zero level set of the shape function $\hat{\phi}$ extracted from the PCA process. The function $\hat{\phi}$ defines an image partioned into two regions Ω_{in} and Ω_{out}, representing respectively the object and the background, whose common boundary is $\hat{C}$:

$$\left\{ \begin{array}{l} \Omega_{in}(\mathbf{x}_{pca}, \mathbf{x}_T) = \{x \in \Omega \mid \hat{\phi}(x, \mathbf{x}_{pca}, \mathbf{x}_T) > 0\}, \\ \Omega_{out}(\mathbf{x}_{pca}, \mathbf{x}_T) = \{x \in \Omega \mid \hat{\phi}(x, \mathbf{x}_{pca}, \mathbf{x}_T) < 0\}, \\ \hat{C}(\mathbf{x}_{pca}, \mathbf{x}_T) = \{x \in \Omega \mid \hat{\phi}(x, \mathbf{x}_{pca}, \mathbf{x}_T) = 0\}. \end{array} \right. \tag{34}$$

The minimization of F_{region} determines the shape parameters $\mathbf{x}_{pca}$ and the parameters $\mathbf{x}_T$ of the rigid or affine transformation of the contour $\hat{C}$ which captures a region having the shape of interest. In our work, we have not considered the smoothing term, $\oint_{\hat{C}} ds$, since shapes generated by the PCA are smooth enough. The functional F_{region} can be written with the shape function $\hat{\phi}$:

$$\begin{array}{c} F_{region}(\mathbf{x}_{pca}, \mathbf{x}_T, u_{in}, u_{out}) = \\ \int_{\Omega} \Theta_{in} H(\hat{\phi}(\mathbf{x}_{pca}, \mathbf{x}_T) d\Omega + \\ \int_{\Omega} \Theta_{out} H(-\hat{\phi}(\mathbf{x}_{pca}, \mathbf{x}_T) d\Omega, \end{array} \tag{35}$$

where $H(.)$ is the Heaviside function, $\Theta_r = |I - u_r|^2 + \mu |\nabla u_r|^2$ and $r = in$ or out.
The modified MS functional (35) is minimized using the gradient descent method for $\mathbf{x}_{pca}$ and $\mathbf{x}_T$ and solving the Euler-Lagrange equations for u_{in} and u_{out}:

$$\left\{ \begin{array}{l} d_t \mathbf{x}_{pca}(t) = \int_{\Omega} (\Theta_{in} - \Theta_{out}) \frac{\partial \hat{\phi}}{\partial \mathbf{x}_{pca}} \, \delta(\hat{\phi}) d\Omega, \\ \qquad\qquad = \int_{\Omega} (\Theta_{in} - \Theta_{out}) \nabla_{\mathbf{x}_{pca}} \hat{\phi} \, \delta(\hat{\phi}) d\Omega, \\ \qquad\quad \text{in }]0, \infty[\times \Omega_{pca}, \\ \mathbf{x}_{pca}(t = 0) = \mathbf{x}_{pca_0} \text{ in } \Omega_{pca}, \end{array} \right. \tag{36}$$

$$\left\{ \begin{array}{l} d_t \mathbf{x}_T(t) = \int_{\Omega} (\Theta_{in} - \Theta_{out}) \frac{\partial \hat{\phi}}{\partial \mathbf{x}_T} \, \delta(\hat{\phi}) d\Omega, \\ \qquad\quad = \int_{\Omega} (\Theta_{in} - \Theta_{out}) \\ \quad \langle \nabla \hat{\phi}, \nabla_{\mathbf{x}_T} h_{\mathbf{x}_T} \rangle \, \delta(\hat{\phi}) d\Omega, \text{ in }]0, \infty[\times \Omega_T, \\ \mathbf{x}_T(t = 0) = \mathbf{x}_{T_0} \text{ in } \Omega_T, \end{array} \right. \tag{37}$$

$$\left\{ \begin{array}{l} \partial_t u_{in}(t, x) = u_{in} - I - \mu \Delta u_{in} \\ \qquad\qquad \text{in }]0, \infty[\times \{\hat{\phi} > 0\}, \\ u_{in}(0, x) = I \text{ in } \{\hat{\phi} > 0\}, \\ \\ \partial_t u_{out}(t, x) = u_{out} - I - \mu \Delta u_{out} \\ \qquad\qquad \text{in }]0, \infty[\times \{\hat{\phi} < 0\}, \\ u_{out}(0, x) = I \text{ in } \{\hat{\phi} < 0\}. \end{array} \right. \tag{38}$$

Figure 17 shows that the minimization of F_{region} segments objects of interest when a part of information is missing and in presence of noise and occlusion. This model can also be used to segment the left brain ventricle on Figure 18.

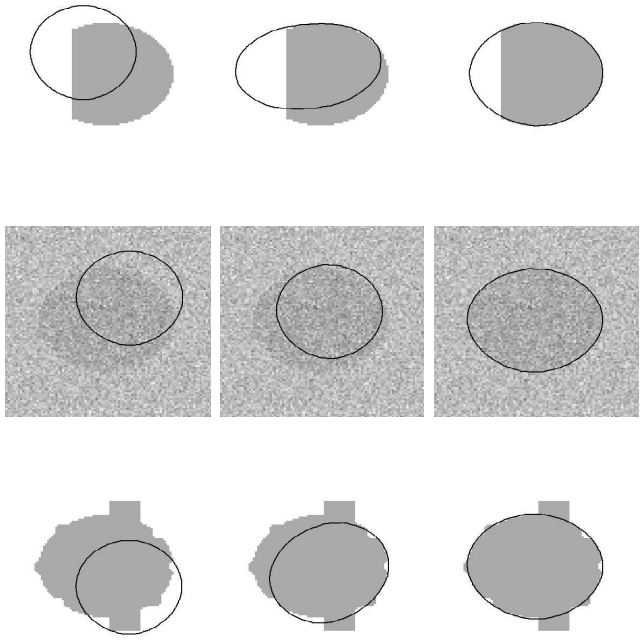

(i)

Fig. 17. Minimization of F_{region} with the flows given by Equations (36-38). The first row presents the evolution of the segmentation process of an ellipse partially cut. The second row shows the segmentation of a noisy ellipse. And the third row is the segmentation of an occluded ellipse.

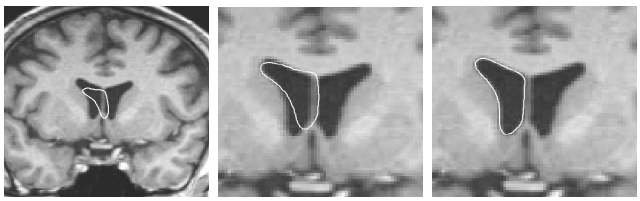

Fig. 18. Segmentation of the left ventricle with the flows given by Equations (36-38).

However, this segmentation method can not handle local structure variations (see Figure 17(i)) when e.g. an ellipse presents irregular boundaries. The model has not captured the local edge variations since it only deals with *global* shape variations provided by the PCA model. If we want to to be able to capture the local variations around the global shape we found, we need to add a local criteria to our energy functional. We will consider for this purpose the classic geodesic active contour given by $F_{boundary}$.
Note that another segmentation method based on the Mumford-Shah functional and the PCA model of Leventon *et al.* has been proposed by Tsai *et al.* [33] for a reduced version of the MS model. Indeed, they have employed the piecewise constant case of the MS functional, proposed by Chan and Vese in [17], whereas we have considered here the general case using the piecewise smooth approximation from [18]. The piecewise smooth case of the MS model enables us to remove the intensity bias present in the piecewise constant case due to the inhomogeneity of the outside region, i.e. the background, with respect to the inside region, the object of interest. This bias affects the computation of the parameters $\mathbf{x}_{pca}$ and $\mathbf{x}_T$.

4.2. Combining Shape-Based, Boundary-Based and Region-Based Functionals

In Section 3.2, we have studied a shape-based functional F_{shape} that evaluates the similarity between the active contour shape and the object shape prior to be segmented. In Section 4.1, we have analysed a region-based functional F_{region} which allows us to drive globally the shape prior towards a homogeneous intensity region. We now combine these two functionals with the boundary-based functional $F_{boundary}$ which captures the object edges to obtain a functional F_2 to segment objects with a statistical shape model and with global and local image information.
The energy minimization of F_2 is performed using the calculus of variations and the gradient descent method. We obtain a system of coupled evolution equations whose steady-state solution gives the minimum of F_2, which means the solution of the segmentation problem. The existence of a minimum of F_2 is proved in annex.
The functional F_2 is expressed in the Eulerian/level set framework as follows:

$$F_2 = \int_\Omega f(x, \mathbf{x}_{pca}, \mathbf{x}_T)|\nabla\varphi|\delta(\varphi)d\Omega + \beta_r \int_\Omega \left(\Theta_{in} H(\hat{\phi}(\mathbf{x}_{pca}, \mathbf{x}_T)) + \Theta_{out} H(-\hat{\phi})\right) d\Omega. \tag{39}$$

And the evolution equations minimizing F_2 are:

$$\begin{cases} \partial_t\varphi(t,x) = \left(f\kappa - \langle\nabla f, \frac{\nabla\varphi}{|\nabla\varphi|}\rangle\right)\delta(\varphi) \\ \qquad\qquad \text{in }]0,\infty[\times\Omega, \\ \varphi(0,x) = \varphi_0(x) \text{ in } \Omega, \\ \frac{\delta(\varphi)}{|\nabla\varphi|}\partial_{\mathcal{N}}\varphi = 0 \text{ on } \partial\Omega, \end{cases} \tag{40}$$

$$\begin{cases} d_t\mathbf{x}_{pca}(t) = -\int_\Omega \nabla_{\mathbf{x}_{pca}}\hat{\phi}(2\beta_s\hat{\phi}|\nabla\varphi|\delta(\varphi)+ \\ \quad \beta_r(\Theta_{in} - \Theta_{out})\delta(\hat{\phi}))d\Omega \text{ in }]0,\infty[\times\Omega_{pca}, \\ \mathbf{x}_{pca}(t=0) = \mathbf{x}_{pca_0} \text{ in } \Omega_{pca}, \end{cases} \tag{41}$$

$$\begin{cases} d_t\mathbf{x}_T(t) = -\int_\Omega \langle\nabla\hat{\phi}, \nabla_{\mathbf{x}_T} h_{\mathbf{x}_T}\rangle \\ \quad (2\beta_s\hat{\phi}|\nabla\varphi|\delta(\varphi)+ \\ \quad \beta_r(\Theta_{in} - \Theta_{out})\delta(\hat{\phi}))d\Omega \text{ in }]0,\infty[\times\Omega_T, \\ \mathbf{x}_T(t=0) = \mathbf{x}_{T_0} \text{ in } \Omega_T, \end{cases} \tag{42}$$

$$\begin{cases} \partial_t u_{in}(t,x) = u_{in} - I - \mu\Delta u_{in} \\ \qquad\qquad \text{in }]0,\infty[\times\{\hat{\phi} > 0\}, \\ u_{in}(0,x) = I \text{ in } \{\hat{\phi} > 0\}, \\ \\ \partial_t u_{out}(t,x) = u_{out} - I - \mu\Delta u_{out} \\ \qquad\qquad \text{in }]0,\infty[\times\{\hat{\phi} < 0\}, \\ u_{out}(0,x) = I \text{ in } \{\hat{\phi} < 0\}. \end{cases} \tag{43}$$

4.3. Implementation Issues

The minimization of F_2 with the evolution equations (40) to (43) are numerically solved by iterating the following stages until convergence is reached:

1. Computation of the shape function $\hat{\phi}(\mathbf{x}_{pca}, \mathbf{x}_T)$ using Equation (7) and performing the rigid and affine transformations (scaling, rotation, translations and shearing) with the B-splines interpolation method [43].

2. Calculation of the gradient $\nabla\hat{\phi}$ using a central difference sheme. The term $\nabla_{\mathbf{x}_{pca}}\hat{\phi}$ is given by the eigenvectors of the PCA model and $\nabla_{\mathbf{x}_T} h_{\mathbf{x}_T}$ is computed according to Equations (22) and (23).

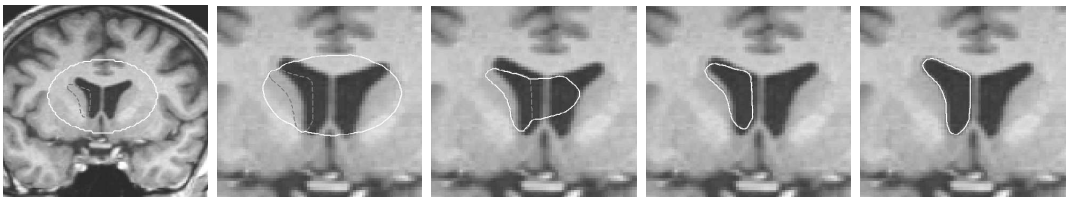

(a) (b) (c) (d) (e)

Fig. 19. Segmentation of the left ventricle by minimizing the functional F_2 with the flows (40) to (43).

3. Discretization of terms $|\nabla\varphi|$ and $\langle\nabla f, \frac{\nabla\varphi}{|\nabla\varphi|}\rangle$ with the Osher-Sethian numerical scheme [11]. Computation of the curvature with central difference schemes. The Dirac function δ and the Heaviside function H are computed by slightly regularized versions following [42, 25].
4. Functions u_{in} and u_{out} are computed in $\{\hat{\phi} > 0\}$ and $\{\hat{\phi} < 0\}$ with the method proposed in [18].
5. Calculation of the temporal derivative using a forward difference approximation.
6. Redistancing the level set function at every iteration with the Fast Marching Method of Adalsteinsson and Sethian [44].

4.4. Experimental Result

We have used our complete segmentation model to segment the left ventricle. Figure 19 presents the evolving active contour with a shape prior by choosing $\beta_s = 2$, $\beta_b = 1$, $\beta_r = 1/10$, $\mu = 3$ and $\Delta t = 0.4$. We get the same result than in section 3.5.2 (Figure 16). However, the convergence towards the solution is faster with the functional F_{region} since more image information is taken into account. Observe the difference between the Figure 16(d) and Figure 19(d). In the first figure, the boundary-based force is weaker than the shape-based force, so the active contour does not stay on the border and go inside the ventricle. Whereas in the second figure, the region-based information allows us to drive the shape prior directly towards the boundaries of the homogeneous region of interest.
Figure 19 illustrates the Section 4.1 remark: in this case, the Mumford-Shah model applied on the active contour will separate both ventricles (that form a homogeneous intensity region) from the rest of the white matter. The shape force will be then opposed to the region force since the shape force will pull the active contour inside the right ventricle towards the left ventricle whereas the Mumford-Shah force will constrain the active contour to stay on the border of ventricles. Our model avoids this situation since region-based forces are only applied on the contour of the shape prior and not on the active contour itself.

5. DISCUSSION

The active contour obtained from the minimization of the energy functional defined in Equation (39) is able to capture high image gradients and a homogeneous intensity region whose shape matches the object of interest. We have seen on Figures 12 and 14 that the shape information allows us to solve the problems of missing information/occlusion while being sensitive to local shape variations. Indeed, small deformations are allowed around the zero level set of the shape function on a distance that depends on the relative weight β_s/β_b. These complex deformations are easier to handle in the level set framework, thanks to its intrinsic representation, than parametric ones [36, 37].
As we mentioned previously, the proposed segmentation model can be seen either as an extension of the model of Chen *et al.* [25] where we have introduced the statistical shape model of Leventon *et al.* [22] and the Mumford-Shah model [18] or as an energy formulation of the model of Leventon *et al.* with the MS energy functional. Using the variational formulation of Chen *et al.* enables us to prove the existence of a solution minimizing our energy functional in the space of functions with bounded variation (see appendix).
Note that the region term based on the Mumford-Shah functional increases the speed of convergence towards the

solution and it also improves the robustness of the model w.r.t. the initial condition, noise and complex background. The PCA shape model we use in our segmentation method presents a good compromise when compared to other models. First, the computation of the p principal components which are orthonormal basis functions is straightforward and fast, using the singular values decomposition method. These functions are then used to produce new shapes of the object of interest according to a simple linear equation. The number p of principal components, i.e. the number of the shape model parameters, is often small as we have noticed for the ellipse (see Figure 3) that needs only one principal component or for the left brain ventricle (see Figure 5) with three principal components. Thus, global shape variations are modeled by a small number of variables which greatly reduces the complexity of the problem, when compared e.g. to Paragios *et al.* model [23]. Indeed, their shape model generates more complex shapes than the PCA but the p shape parameters of the PCA model is replaced in their work by a local deformation field to be evaluated on a δ-band around the zero level set of the shape function. Note that the shapes produced by the PCA are obviously implicit and intrinsic, i.e. independant of the parametrization, which facilitates the morphing and the registration processes. However, shape functions provided by the PCA are not exactly SDFs as proven by Leventon in [22, 32]. Nevertheless, shape functions of the PCA are very close to SDFs, which allow us to use them in practice. New shape functions must actually satisfy the following condition to be successfully used in the morphing and the registration processes: a point belonging to the shape function must see its intensity continuously decreasing when moving towards the zero level set even if its gradient is not exactly in the normal direction of the zero level set. The shape functions generated by the PCA model satisfy this condition. Moreover, the previous condition also allows us to use affine transformations since the affinely transformed SDFs still satisfy this condition.
The shape functions given by the PCA are thus not accurate SDFs but there are two ways to obtain exact SDFs (and have a strict equality in Equation (14)). Either the shape function is projected in the SDFs space by redistancing $\hat{\phi}$ as a SDF or the framework of Charpiat *et al.* [24] can be used to define a mean and principal modes of variation for distance functions.
In our segmentation model, we have to compute the transformation and shape parameters. However, Cremers *et al.* in [36, 37] have defined two shape energies independant of the rigid transformations and the shape parameters. This means that their segmentation model had not to compute the vector of the rigid transformations $\mathbf{x}_T$ and the vector of shape parameters $\mathbf{x}_{pca}$. Thus, is it really useful to estimate the registration parameters $\mathbf{x}_T$ and the shape parameters $\mathbf{x}_{pca}$? It depends on two questions: does the current application need to compute transformation and shape parameters and are affine or non-rigid transformations necessary? If the answer is positive for one of these questions, the estimation of these parameters will be imperative. In [25, 45] for example, the transformation parameters are used to align time series images in order to minimize the effect of motion on the fMRI signal. Then, the shape vector $\mathbf{x}_{pca}$ can be useful to know the probability that the segmented object belongs to its training set. Finally, since we are using a variational framework and the PDEs attached to it, we can consider other models such as [19] to segment objects by linearly combining energy functionals or the PDEs directly.

6. CONCLUSION

In this paper, we have proposed a new variational method to solve the fundamental problem of object segmentation using local and global image information with a geometric shape prior given by the statistical model of PCA. To reach this objective, we have defined in Section 3.2 a shape-based functional to force the active contour to get a shape of interest whatever the position of the active contour in the image. Then in Section 4.1, we have proposed a Mumford and Shah-based functional to drive globally the shape model towards a homogeneous intensity region with the shape of interest. Experimental results have shown that our active contour is able to solve the problems of missing information and occlusion while being sensitive to local shape variations.
The statistical shape model we used is the PCA model. As explained in Section 5, this model presents a good compromise between low complexity and acceptable shape priors. However, this model works well only if the probability density function (PDF) of the training set of the object of interest is Gaussian. If the true underlying PDF of the training set is not Gaussian (in presence of tumors in T1-WMR images for example) then more elaborated techniques such as non-parametric models are necessary.
Finally, note that the proposed model can capture only one object, which is a strong limitation since we loose the powerful property of the level set approach that can segment several objects simultaneously. A first solution to handle multiple objects would consist in associating structures by coupling the evolution equations.

Appendix: Existence of a Solution For our Minimization Problem

This section deals with the mathematical study of

$$\min_{\varphi,\mathbf{x}_{pca},\mathbf{x}_T,u_{in},u_{out}} \{F_2 = \int_\Omega \left(\beta_b g(x) + \beta_s \hat{\phi}^2(x,\mathbf{x}_{pca},\mathbf{x}_T)\right) |\nabla H(\varphi)| + \beta_r F_{region}(\mathbf{x}_{pca},\mathbf{x}_T,u_{in},u_{out})\}. \quad (44)$$

We follow the proofs of Chen *et al.* in [25] and Vese and Chan [46] to prove the existence of a minimizer for our proposed minimization problem using the direct method of the calculus of variations and compactness theorems on the space of functions with bounded variation.
The minimization problem is considered among characteristic functions χ_E of sets $E = \{x \in \Omega | \varphi(x) \geq 0\}$ with bounded variation. The vector of PCA eigencoefficients $\mathbf{x}_{pca} = (\mathbf{x}_{pca_1}, ..., \mathbf{x}_{pca_p})$ is defined on $\Omega_{pca} = [-3\lambda_1, 3\lambda_1] \times ... \times [-3\lambda_p, 3\lambda_p]$ and the vector of geometric transformations $\mathbf{x}_T = (s_x, s_y, \theta, s_h, T_x, T_y)$ is defined on Ω_T. If $\Omega \subset \mathbf{R}^2$ is the domain of the original image I, say $\Omega = (0,255)^2$, then $\Omega_T = (0,255]^2 \times [-\pi,\pi) \times [-127,127] \times [-255,255]^2$. Functions u_{in} and u_{out} from Section 4.1 are supposed in $C^1(\Omega)$ since they are smoothed versions of the original image u_0 ($u = u_0 + \mu\Delta u$ is the first order discretization of the linear heat diffusion equation $\partial_t u = \Delta u$ with $u(0) = u_0$).

We remind some definitions and theorems introduced in Evans and Gariepy [2], Giusti [3], Chen [25], Chan and Vese [46] and Ambrosio [47].

Definition 1: Let $\Omega \subset \mathbf{R}^N$ be an open set and let $f \in L^1(\Omega)$. The total variation norm of f is defined by

$$TV(f) = \int_\Omega |\nabla f| = \sup_{\phi \in \Phi} \left\{ \int_\Omega f(x) \text{div } \phi(x) \right\}, \quad (45)$$

$$\text{where} \quad \Phi = \left\{ \phi \in C_0^1(\Omega, \mathbf{R}^N) | \ |\phi(x)| \geq 1, \text{on } \Omega \right\}. \quad (46)$$

Definition 2: A function $f \in L^1(\Omega)$ is said to have bounded variation in Ω if its distributional derivate satisfies $TV(f) < \infty$. We define $BV(\Omega)$ as the space of all functions in $L^1(\Omega)$ with bounded variation. The space $BV(\Omega)$ is a Banach space, endowed with the norm:

$$\|f\|_{BV(\Omega)} = \|f\|_{L^1(\Omega)} + TV(f). \quad (47)$$

Theorem 1 *A measurable subset E of $\mathbf{R}^N$ has finite perimeter in Ω if and only if the characteristic function $\chi_E \in BV(\Omega)$. We have $per_\Omega(E) = TV(\chi_E) = \int_\Omega |\nabla \chi_E| < \infty$.*

Definition 3: Let $\Omega \subset \mathbf{R}^N$ be an open set and let $f \in L^1(\Omega)$ and $\alpha(x)$ be positive valued continuous and bounded functions on Ω. The weighted total variation norm of f is defined by

$$TV_\alpha(f) = \int_\Omega \alpha(x)|\nabla f| = \sup_{\phi \in \Phi_\alpha} \left\{ \int_\Omega f(x) \text{div } \phi(x) \right\}, \quad (48)$$

where

$$\Phi_\alpha = \left\{ \phi \in C_0^1(\Omega, \mathbf{R}^N) | \ |\phi(x)| \geq \alpha(x), \text{on } \Omega \right\}. \quad (49)$$

If a function f has a finite weighted total variation norm in Ω then it also belongs to $BV(\Omega)$.

Definition 4: A function $f \in BV(\Omega)$ is a special function of bounded variation if its distributional derivative is given by

$$|Df| = TV(f) + \int_{\Omega \cap S_f} J_f d\mathcal{H}^{N-1}, \quad (50)$$

where J_f is the jump part defined on the set of points S_f and $\mathcal{H}^{N-1}$ is the (N-1)-dimensional Hausdorff measure. The space of special functions of bounded variation $SBV(\Omega)$ is a Banach space, endowed with the norm:

$$\|f\|_{SBV(\Omega)} = \|f\|_{L^1(\Omega)} + |Df|. \tag{51}$$

Theorem 2 *Let $\Omega \subset \mathbf{R}^N$ be an open set with a Lipschity boundary. If $\{f_n\}_{n\geq 1}$ is a bounded sequence in $BV(\Omega)$, then there exist a subsequence $\{f_{n_j}\}$ of $\{f_n\}$ and a function $f \in BV(\Omega)$, such that $f_{n_j} \to f$ strongly in $L^p(\Omega)$ for any $1 \leq p < N/(N-1)$ and*

$$TV(f) \leq \underset{n_j \to \infty}{lim\ inf}\, TV(f_{n_j}). \tag{52}$$

The following theorem is a generalization of the **main theorem** of Chen [25].

Theorem 3 *Let $\Omega \subset \mathbf{R}^N$ be an open set with a Lipschity boundary. If $\{f_n\}_{n\geq 1}$ is a bounded sequence in $BV(\Omega)$ and if $\{\alpha_n\}_{n\geq 1}$ is a sequence of positive valued continuous functions that uniformly converges to α on Ω, then there exist subsequences $\{f_{n_j}\}$ of $\{f_n\}$ and a function $f \in BV(\Omega)$ such that $f_{n_j} \to f$ strongly in $L^p(\Omega)$ for any $1 \leq p < N/(N-1)$ and*

$$TV_\alpha(f) \leq \underset{n_j \to \infty}{lim\ inf}\, TV_{\alpha_{n_j}}(f_{n_j}). \tag{53}$$

Theorem 4 *Let Ω be a bounded and open subset of $\mathbf{R}^2$ and I be a given image with $I \in L^\infty(\Omega)$. The minimization problem (44) re-writes in the following form*

$$\begin{aligned} \min_{\chi_E, \mathbf{x}_{pca}, \mathbf{x}_T, u_{in}, u_{out}} \{F_2 = \\ \int_\Omega \left(\beta_b g(x) + \beta_s \hat{\phi}^2(x, \mathbf{x}_{pca}, \mathbf{x}_T)\right) |\nabla \chi_E| + \\ \beta_r F_{region}(\mathbf{x}_{pca}, \mathbf{x}_T, u_{in}, u_{out})\} \end{aligned} \tag{54}$$

has a solution $\chi_E \in BV(\Omega)$, $\mathbf{x}_{pca} \in \Omega_{pca}$, $\mathbf{x}_T \in \Omega_T$ and u_{in}, $u_{out} \in C^1(\Omega)$.

Proof: We use the direct method of the calculus of variations:
(A) Let $\{\chi_{E_n}, \mathbf{x}_{pca_n}, \mathbf{x}_{T_n}, u_{in_n}, u_{out_n}\}_{n\geq 1}$ be a minimizing sequence of (54), i.e.

$$\begin{aligned} \lim_{n\to\infty} F_2(\chi_{E_n}, \mathbf{x}_{pca_n}, \mathbf{x}_{T_n}, u_{in_n}, u_{out_n}) = \\ \inf_{\chi_E, \mathbf{x}_{pca}, \mathbf{x}_T, u_{in}, u_{out}} F(\chi_E, \mathbf{x}_{pca}, \mathbf{x}_T, u_{in}, u_{out}). \end{aligned} \tag{55}$$

(B) Since χ_{E_n} is a sequence of characteristic functions of E_n, then $\chi_{E_n}(x) \in \{0, 1\}$ - a.e. in Ω. A constant $M > 0$ exists such that $\|\chi_{E_n}\|_{L^1(\Omega)} \leq M$, $\forall n \geq 1$. Therefore, χ_{E_n} is a uniformly bounded sequence on $BV(\Omega)$.
Since $\{\mathbf{x}_{pca_n}\}$ and $\{\mathbf{x}_{T_n}\}$ are bounded sequences on compact spaces Ω_{pca} and Ω_T, subsequences that converge to limits $\mathbf{x}_{pca}$ and $\mathbf{x}_T$ exist.
The integrant $f(x, \mathbf{x}_{pca}, \mathbf{x}_T) = \beta_b g + \beta_s \hat{\phi}^2$ is positive and bounded because both functions $\hat{\phi}^2$ and g are bounded on Ω. Since the PCA is applied on continuous functions (SDFs) then the functions $\hat{\phi}$ and f are also continuous and $f_n(\mathbf{x}) = f(\mathbf{x}, \mathbf{x}_{pca_n}, \mathbf{x}_{T_n})$ converges uniformly to f on Ω.
Following Theorem 3, a subsequence of χ_{E_n} that converges to a function χ_E strongly in $L^1(\Omega)$ exists.
Moreover , Theorem 3 also states that

$$\int_\Omega f|\nabla \chi_E| \leq \liminf_{n_j \to \infty} \int_\Omega f_{n_j} |\nabla \chi_{E_{n_j}}|, \tag{56}$$

(C) In the region-based functional defined in Equation (35):

$$\begin{aligned} F_{region}(\mathbf{x}_{pca}, \mathbf{x}_T, u_{in}, u_{out}) = \\ \int_\Omega (\Theta_{in} H(\hat{\phi}(\mathbf{x}_{pca}, \mathbf{x}_T)) + \Theta_{out} H(-\hat{\phi})) d\Omega, \end{aligned} \tag{57}$$

the function $H(\hat{\phi}(\mathbf{x}_{pca}, \mathbf{x}_T))$ is a characteristic function χ_G of sets $G = \{x \in \Omega | \hat{\phi}(x) \geq 0\}$. So we have

$$F_{region}(\mathbf{x}_{pca}, \mathbf{x}_T, u_{in}, u_{out}) = \int_\Omega (\Theta_{in}\chi_G(\mathbf{x}_{pca}, \mathbf{x}_T)) + \Theta_{out}(1 - \chi_G))d\Omega \tag{58}$$

and we can define the function $u = u_{in}\chi_G + u_{out}(1 - \chi_G)$. The minimizing sequence of Equation (54) implies

$$\lim_{n\to\infty} F_{region}(\mathbf{x}_{pca_n}, \mathbf{x}_{T_n}, u_{in_n}, u_{out_n}) = \inf_{\mathbf{x}_{pca}, \mathbf{x}_T, u_{in}, u_{out}} F_{region}(\mathbf{x}_{pca}, \mathbf{x}_T, u_{in}, u_{out}). \tag{59}$$

Since the function χ_G depends continuously on variables $\mathbf{x}_{pca}$ and $\mathbf{x}_T$, we have $\chi_G(\mathbf{x}_{pca_n}, \mathbf{x}_{T_n}) = \chi_{Gn}$ and $u_n = u_{in_n}\chi_{Gn} + u_{out_n}(1 - \chi_{Gn})$. According to Ambrosio's lemna [47], we can deduce that there is a $u \in SBV(\Omega)$, such that a subsequence u_{n_j} converges to u a.e. in $BV - w*$ and

$$F_{region}(\mathbf{x}_{pca}, \mathbf{x}_T, u_{in}, u_{out}) = F_{region}(u) \leq \liminf_{n_j\to\infty} F_{region}(u_{n_j}), \tag{60}$$

which means that u is a minimizer of F_{region}. Then, by combining Equations (56) and (60), χ_E, $\mathbf{x}_{pca}$, $\mathbf{x}_T$, u_{in} and u_{out} are minimizers of (54).

References

[1] M. Crandall, H. Ishi, and P. Lions, "Users' Guide to Viscosity Solutions of Second Order Partial Differential Equations," *Bulletin of the American Mathematic Society*, vol. 27(1), pp. 1–69, 1992.

[2] L. Evans and R. Gariepy, *Measure Theory and Fine Properties of Functions*. Studies in advanced Mathematics, CRC Press, 1992.

[3] E. Giusti, *Minimal Surfaces and Functions of Bounded Variation*. Birkhauser, Basel, 1985.

[4] J. Morel and S. Solimini, *Variational Methods in Image Segmentation*. Progress in Nonlinear Differential Equations and Their Applications, 1995.

[5] J. Sethian, *Level Set Methods and Fast Marching Methods: Evolving Interfaces in Computational Geometry, Fluid Mechanisms, Computer Vision, and Material Sciences.* Cambridge University Press, 1999.

[6] G. Sapiro, *Geometric Partial Differential Equations and Image Processing*. Cambridge University Press, 2001.

[7] G. Aubert and P. Kornprobst, *Mathematical Problems in Image Processing: Partial Differential Equations and the Calculus of Variations*, vol. 147. Springer, 2001.

[8] S. Osher and N. Paragios, *Geometric Level Set Methods in Imaging, Vision and Graphics*. Springer Verlag, 2003.

[9] D. Mumford and J. Shah, "Boundary Detection by Minimizing Functionals," in *International Conference on Computer Vision and Pattern Recognition*, pp. 22–26, IEEE, 1985.

[10] M. Kass, A. Witkin, and D. Terzopoulos, "Snakes: Active Contour Models," *International Journal of Computer Vision*, pp. 321–331, 1987.

[11] S. Osher and J. Sethian, "Fronts Propagating with Curvature-Dependent Speed: Algorithms Based on Hamilton-Jacobi Formulations," *Journal of Computational Physics*, vol. 79(1), no. 12-49, 1988.

[12] A. Yezzi, S. Kichenassamy, A. Kumar, P. Olver, and A. Tannenbaum, "A Geometric Snake Model for Segmentation of Medical Imagery," *IEEE Transactions on Medical Imaging*, vol. 16(2), pp. 199–209, 1997.

[13] R. Malladi, R. Kimmel, D. Adalsteinsson, G. Sapiro, V. Caselles, and J. Sethian, "A Geometric Approach to Segmentation and Analysis of 3D Medical Images," in *Mathematical Methods in Biomedical Image Analysis Workshop*, 1996.

[14] L. Jonasson, P. Hagmann, X. Bresson, R. Meuli, O. Cuisenaire, and J. Thiran, "White Matter Mapping in DT-MRI using Geometric Flows," in *9th EUROCAST conference on Computer Aided Systems Theory*, 2003.

[15] N. Paragios and R. Deriche, "Geodesic Active Contours and Level Sets for the Detection and Tracking of Moving Objects," *IEEE Transactions on Pattern Analysis and Machine Intelligence*, vol. 22, no. 3, pp. 266–280, 2000.

[16] N. Paragios and R. Deriche, "Coupled Geodesic Active Regions for Image Segmentation: A Level Set Approach," in *European Conference of Computer Vision, 224-240*, pp. 224–240, 2000.

[17] T. Chan and L. Vese, "Active Contours without Edges," *IEEE Transactions on Image Processing*, vol. 10(2), pp. 266–277, 2001.

[18] T. Chan and L. Vese, "A Multiphase Level Set Framework for Image Segmentation Using the Mumford and Shah Model," *International Journal of Computer Vision*, vol. 50(3), pp. 271–293, 2002.

[19] S. Jehan-Besson, M. Barlaud, and G. Aubert, "DREAM2S: Deformable Regions Driven by an Eulerian Accurate Minimization Method for Image and Video Segmentation," *Technical Report RR 2001-14, Laboratoire I3S*, 2001.

[20] G. Aubert, M. Barlaud, O. Faugeras, and S. Jehan-Besson, "Image Segmentation Using Active Contours: Calculus of Variations of Shape Gradients," *Research Report RR 4483, INRIA*, July 2002.

[21] T. Cootes and C. Taylor, "Statistical Models of Appearance for Computer Vision, Technical report, University of Manchester," 1999.

[22] M. Leventon, W. Grimson, and O. Faugeras, "Statistical Shape Influence in Geodesic Active Contours," in *International Conference of Computer Vision and Pattern Recognition*, pp. 316–323, 2000.

[23] N. Paragios, M. Rousson, and V. Ramesh, "Non-rigid Registration using Distance Functions," *Journal of Computer Vision and Image Understanding*, vol. 89, pp. 142–165, 2003.

[24] G. Charpiat, O. Faugeras, and R. Keriven, "Shape Metrics, Warping and Statistics," in *International Conference on Image Processing*, pp. 627–630, 2003.

[25] Y. Chen, H. Tagare, S. Thiruvenkadam, F. Huang, D. Wilson, K. Gopinath, R. Briggsand, and E. Geiser, "Using Prior Shapes in Geometric Active Contours in a Variational Framework," *International Journal of Computer Vision*, vol. 50(3), pp. 315–328, 2002.

[26] V. Caselles, R. Kimmel, and G. Sapiro, "Geodesic Active Contours," *International Journal of Computer Vision*, vol. 22(1), pp. 61–79, 1997.

[27] S. Kichenassamy, A. Kumar, P. Olver, A. Tannenbaum, and A. Yezzi, "Gradient Flows and Geometric Active Contour Models," in *International Conference on Computer Vision*, pp. 810–815, IEEE, June 1995.

[28] S. Kichenassamy, A. Kumar, P. Olver, A. Tannenbaum, and A. Yezzi, "Conformal Curvature Flows: From Phase Transitions to Active Vision," in *Archive for Rational Mechanics and Analysis*, vol. 134, pp. 275–301, 1996.

[29] M. Delfour and J. Zolésio, *Shapes and Geometries: Analysis, Differential Calculus, and Optimization*. Advances in Design and Control 4, SIAM, 2001.

[30] J. Sokolowski and J. Zolésio, *Introduction to Shape Optimization : Shape Sensitivity Analysis*. Volume 16 of Springer series in computational mathematics, Springer-Verlag, 1992.

[31] A. Tsai, J. Yezzi, and A. Willsky, "Curve Evolution Implementation of the Mumford-Shah Functional for Image Segmentation, Denoising, Interpolation and Magnification," *IEEE Transactions on Image Processing*, vol. 10(8), pp. 1169–1186, 2001.

[32] M. Leventon, "Statistical Models for Medical Image Analysis, Ph.D Thesis," 2000.

[33] A. Tsai, A. Yezzi, W. Wells, C. Tempany, D. Tucker, A. Fan, W. Grimson, and A. Willsky, "Model-based Curve Evolution Techniques for Image Segmentation," in *Conference on computer vision and pattern recognition*, pp. 463–468, 2001.

[34] Y. Chen, S. Thiruvenkadam, H. Tagare, F. Huang, D. Wilson, and E. Geiser, "On the Incorporation of Shape Priors into Geometric Active Contours," in *Workshop on Variational and Level Set Methods in Computer Vision*, pp. 145–152, 2001.

[35] N. Paragios and M. Rousson, "Shape Priors for Level Set Representations," in *European Conference in Computer Vision, Copenhagen, Denmark*, 2002.

[36] D. Cremers, F. Tischhäuser, J. Weickert, and C. Schnörr, "Diffusion Snakes: Introducing Statistical Shape Knowledge into the Mumford-Shah Functional," *International Journal of Computer Vision*, vol. 50(3), pp. 295–313, 2002.

[37] D. Cremers, T. Kohlberger, and C. Schnorr, "Nonlinear Shape Statistics in Mumford-Shah Based Segmentation," in *European Conference on Computer Vision*, pp. 93–108, 2002.

[38] D.Cremers, "Statistical Shape Knowledge in Variational Image Segmentation, Ph.D Thesis," 2003.

[39] L. Davis, *Handbook of Genetic Algorithms*. Van Nostrand, 1991.

[40] *Numerical Recipies in C++ and C*. Cambridge University Press.

[41] X. Bresson, P. Vandergheynst, and J. Thiran, "A Priori Information in Image Segmentation: Energy Functional Based on Shape Statistical Model and Image Information," in *International Conference on Image Processing*, pp. 425–428, 2003.

[42] H. Zhao, T. Chan, B. Merriman, and S. Osher, "A Variational Level Set Approach to Multiphase Motion," *Journal of Computational Physics*, vol. 127, pp. 179–195, 1996.

[43] M. Unser, "Splines: A Perfect Fit for Signal and Image Processing," *IEEE Signal Processing Magazine*, vol. 16(6), pp. 22–38, 1999.

[44] D. Adalsteinsson and J. Sethian, "A Fast Level Set Method for Propagating Interfaces," *Journal of Computational Physics*, vol. 118, pp. 269–277, 1995.

[45] B. Biswal and J. Hyde, "Contour-based Registration Technique to Differentiate Between Task-activated and Head Motion-induced Signal Variations in fMRI," *Magnetic Resonance in Medecine*, vol. 38(3), pp. 470–476, 1997.

[46] L. Vese and T. Chan, "A Multiphase Level Set Framework for Image Segmentation Using the Mumford and Shah Model, UCLA CAM Report 01-25," 2001.

[47] L. Ambrosio, "A Compactness Theorem for a New Class of Functions of bounded variation," *Bolletino Della Unione Matematica Italiana*, vol. VII(4), pp. 857–881, 1989.